energies

MDPI

Article

Trough-Type Free-Form Secondary Solar Concentrator for CPV/T Application

Xian-long Meng [1,2,*], Fu-Peng Ren [3], Peng Zhang [1] and Zi-xuan Tang [1]

[1] School of Power and Energy, Northwestern Polytechnical University, Xi'an 710072, China
[2] Yangtze River Delta Research Institute of NPU, Northwestern Polytechnical University, Taicang 215400, China
[3] Harbin Dongan Automotive Engine Manufacturing Co., Harbin 150060, China
* Correspondence: mengxl@nwpu.edu.cn; Tel.: +86-181-8261-9721

Abstract: Imaging concentrators like the parabolic trough solar concentrators have been widely employed for energy production in solar power plants. The conventional imaging solar concentrators form a non-uniform Gaussian distribution on receiving absorbers yielding the highest temperatures. The traditional CSP system normally truncated a peripheral region of heat flux to better use the central part. CPV/T systems using the waste heat recovery method can largely improve the total efficiency. However, for the CPV module, the coolant temperature was usually below 80 °C, which limited the applications of the thermal cycle such as the ORC system. In this article, a novel trough-type free-form secondary solar concentrator (TFSC) for PV/Thermal hybrid application has been proposed. Different from other CPV/T concepts using a combined PV panel and cooling tunnel/tube, the current concept separates the receiver in two parts. The secondary free-form reflector is generated by the geometric construction method, resulting in uniform heat flux in the edge region and high concentration in the central region. Through the ray tracing method, the optical properties have been verified. Sensitivity analysis of the concentrating structure is also conducted. The results provide supports for the design and applications of novel CPV/T systems.

Keywords: solar concentrator; solar power; CPV/T; free-form optics; ray tracing

Citation: Meng, X.-l.; Ren, F.-P.; Zhang, P.; Tang, Z.-x. Trough-Type Free-Form Secondary Solar Concentrator for CPV/T Application. *Energies* **2022**, *15*, 8023. https://doi.org/10.3390/en15218023

Academic Editors: Yong Shuai and Bachirou Guene Lougou

Received: 10 October 2022
Accepted: 20 October 2022
Published: 28 October 2022

1. Introduction

1.1. Research Background of CSP

Solar energy offers a valuable solution to the challenges facing energy security and also plays an important role in the reduction of global warming. Solar concentrators are key components for Concentrated Solar Power (CSP) that allows a smaller area to collect a large mass of solar rays for the heat transfer or electricity generation [1]. For thermal heat transfer, this will increase the grade of power as well as the thermodynamic cycle. For electrical use, the so-called Concentrated Photovoltaics (CPV) systems can be the answer to reducing the cost of solar power, but they are also more environmentally friendly than regular flat-plate PV panels. Scientists made every effort to achieve higher conversion and installed capacity of CSP systems.

However, the conventional imaging solar concentrators normally obtain a Gaussian distribution on receiving absorber that few studies fully utilized, as shown in Figure 1. The concentrated heat flux decreases significantly at a higher radius. Previously, the receiver was constantly truncated for practical application to keep the central part of high concentration [2], because a smaller receiving size is able to achieve lower radiation loss and higher pressure capacity. The corresponding incident angles become lower and can increase the radiation absorptions by the receivers as well. Another reason to truncate the edge heat flux is that solar power is, after all, a free energy source that can be discarded in a certain extent. This will no doubt inevitably decrease optical efficiency.

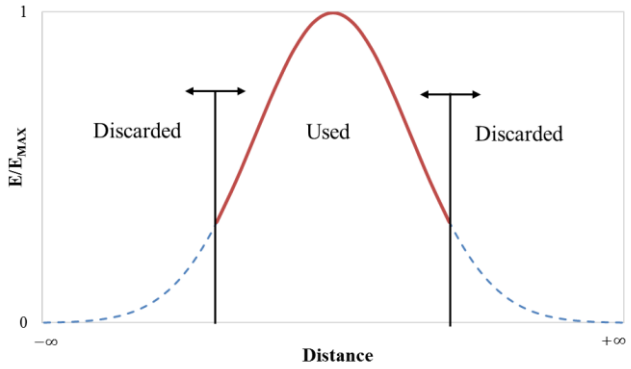

Figure 1. Gaussian distribution received by traditional imaging concentrators.

1.2. Research Progress in CPV and CPV/T Technologies

Previously, exploratory studies about non-imaging optical devices developing for better utilization of discarded heat flux have been started. Compound Parabolic Concentrator (CPC), a typical non-imaging concentrator that obtains a wide acceptance angle, has been used as the secondary mirror fitting with a primary dish concentrator to obtain a higher concentration than a single dish [3]. A tailored edge-ray concentrator (TERC) assembled with a primary fresnel concentrator [4] or dish concentrator [5] has also been developed for maximum solar concentration. Another interesting idea is to arrange a partial ring of tubular receivers (preheaters) using pentagon concentrators surrounding the central high-temperature stage to reduce the radiation and convection loss [6]. However, all of the above cases were developed for thermal heat transfer.

Except using solar thermal receivers, scientists also applied the CPV module in the central region of the focal plane and circular tube around the peripheral region. It was found that the hybrid system can be always operated with high efficiency despite the DNI change at different moments or days. Through this train of thought, a great number of studies about CPV/T technologies have been reported [7]. The CPV/T technologies mainly include the spectral beam splitting method and waste heat recovery method. The former is widely used in industry and aerospace areas. Different kinds of wave-divided devices were adopted to split solar radiation for fitting the spectral response of the PV cell and leaving the rest for thermal heat transfer. Applied CPV/T systems include linear concentrators (parabolic troughs, linear Fresnel lenses/reflectors, and cylindrical troughs) and point concentrators (parabolic dish and heliostat-tower), etc. For the waste heat recovery method, the CPV receivers were mounted together with the heat exchanger for both the thermal heat transfer and electricity. The active cooling module would improve the PV efficiency while also producing hot water for heating, absorptive cooling, etc. Few CPV/T systems separated thermal and electrical functions in one concentrating system.

Optical irradiance is another important factor affecting CPV systems. For a PV panel, the current mismatching phenomenon results in the decrease of the Fill Factor and PV conversion efficiency. This will be even enhanced at a high concentration and leads to local overheating, which further decreases the output efficiency and lifetime. In order to improve the heat flux uniformity, most previous studies adopted non-imaging optical systems such as total reflection homogenizer [8], overlapped multi surfaces [9] or free-form optical modules [10]. Free-form optics have been introduced to the CSP area in recent years. A free-form surface does not have a certain mathematical expression which consists of several curved surfaces, for instance, B-spline patches [11]. Hence, this technology has higher freedom in its design process, which can be applied in the precise control of energy transmission. For improving the efficiency, compactness and error tolerance, free-form optics are widely adopted in Concentrating Photovoltaics. The XR-type CPV module is a representative work using the off-axis structure. The optical system consisting of a primary "X" reflector and a secondary "R" lens was designed using the SMS method [12]. The test output efficiency of the assembled module reached 33% at the solar concentration of

1000×. Other CPV modules based on the Köhler lighting principle such as the Fresnel-lens-based FK module [10,13], TIR-R modules [14] and Cassegrain RXI modules [15] have been exploited by the same team. However, there are few studies about the hybrid PV/T applications using the above technologies.

1.3. Intention of Current Study

From the above development status, it can be found that the efficient utilization of concentrated solar radiation is an eternal theme in the CSP area. The traditional CSP system normally truncated the peripheral region of heat flux to better use the central part. The total heat flux was not fully utilized.

In the current study, the total radiation power would be efficiently collected on the receiving surface. Although the waste heat recovery method can largely improve the total efficiency, around the bottom of the CPV module, the temperature of the coolant was usually below 80 °C, which limited the thermal cycle application such as the ORC system. Based on the above considerations, a novel trough free-form solar concentrator for PV/Thermal hybrid application has been proposed. Different from other CPV/T concepts using a combined PV panel and cooling tunnel/tube, the current concept separates the receiver in two parts. The coolant can be firstly used to release the heat from the CPV module and then flow into the heat transfer tunnel. The cooling temperature can be dramatically increased for the heat engine cycle in the solar power station. Besides, free-form optics are applied for improving the uniformity of irradiance on the PV panel.

To decrease the manufacturing cost, the primary concentrator is selected as a classical parabola trough for high solar concentration, and the secondary is a free-form surface for flexible optical adjustment. The secondary free-form reflector is generated by the geometric construction method, resulting in uniform heat flux in the edge region and high concentration in the central region. Through the ray tracing method, the optical properties have been verified. Sensitivity analysis is also conducted. The results provide supports for the design and applications of novel CPV/T systems.

2. System Description

The TFSC system is composed by a two-stage solar concentrator and thermal/electrical combined receivers. In order to save on manufacturing costs, the conventional parabola trough surface that has been commercially produced is used as the primary mirror, and the secondary free-form surface with a much smaller size can be easily processed in practical application. To better utilize the edge aperture of Gaussian heat flux collected by the primary trough concentrator and maximize the heat flux uniformity of the PV panel, the Cassegrain secondary reflector of the TFSC is constructed based on the 2D-GCM method. The current study focuses on the optical performance of a solar-concentrating system, so a flat absorbing surface is replaced to observe the direct receiving heat flux, as shown in Figure 2. The photovoltaic panel receiver (PVR) is arranged along two flanks of TR, which obtains low-concentration and uniform heat flux, wherein a certain space had been reserved for linkage components and optical error tolerance. This factor has been taken into account in the design process, when the preset target mapping had skipped this area to make full use of the collected radiation.

As shown in Figure 2, the optical axis of the primary trough concentrator is arranged coincident with z-axis. Origin O_1 is the parabolic center. The PV and thermal absorber are both arranged along the x-axis at z = 0. O_2 is the focus point of the primary mirror. R_{min} and R_{max} are the inner and outer widths of the primary trough concentrator, respectively. r_{min} is the inner width of the PV receiver, and r_{max} is the outer width.

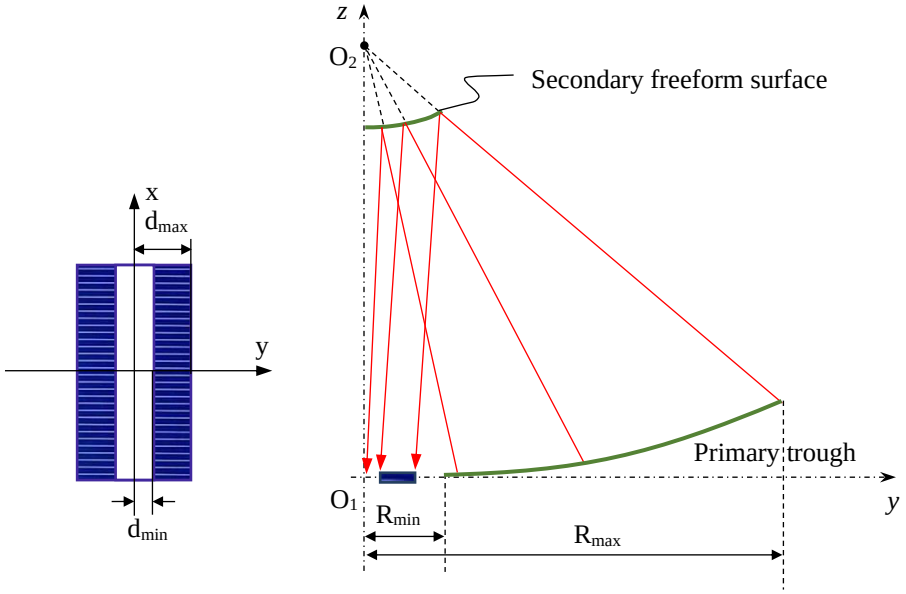

Figure 2. Sketch of the TFSC structure and rim ray tracing.

The combined PV/Thermal receiver can simultaneously achieve high-temperature heat transfer and high-efficiency electricity generation. A trough solar concentrator normally adopts a tube absorber as a Thermal Receiver (TR) component. The coolant can be firstly used to release the heat of the CPV module and then flow into the heat transfer tunnel. Different from traditional CPV/T systems using the waste heat recovery method, as shown in Figure 3, the coolant in the current model is heated in two separated PV and thermal regions instead of a single CPV module. The output medium temperature can be then dramatically increased for the heat engine cycle in a solar power station.

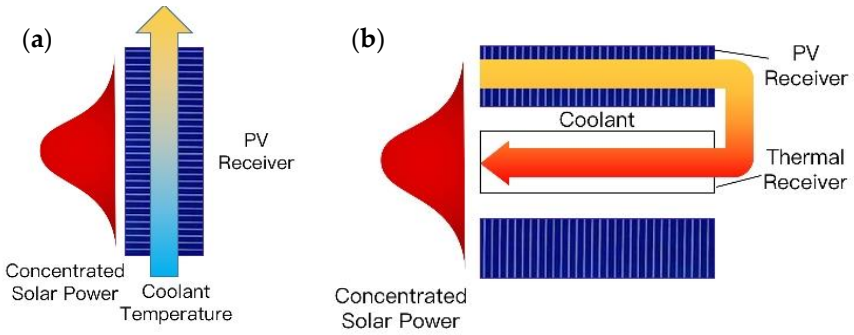

Figure 3. Comparison of CPV/T model coolant, the TFSC. (**a**) Traditional CPV/T model based on waste heat recovery method. (**b**) Novel-type model based on divided heat transfer procedure.

3. Free-Form Surface Generation and Mathematical Model

Free-form optics is a fast-developing technology in illumination engineering [16] and solar energy [17]. A free-form surface does not have a fixed expression so that it possesses an extra-high degree of design freedom. The generation of free-form surface is a key problem that can be solved by various developed methods such as the Wassermann–Wolf differential equation method [18], simultaneous multiple surface method (SMS), etc. The geometric construction method (GCM) directly adopted ray path and the principle of geometrical optics to build the free-form surface that is especially suitable for the known light source and target. However, the traditional GCM has the disadvantage of high surface error. For improving the heat flux uniformity of PV cell C, Tsai developed a free-form concentrator by connecting several circular arc segments together [19]. In the current study, a similar model is extended for a PV/Thermal hybrid system, named the Curved

Geometry Construction Method (CGCM). Particularly, several constraint conditions must be considered and improved to meet both the requirements of point focusing and heat flux uniformity. The solution procedure is based on skew ray tracing and given as follows:

(1) As Figure 4 shows, assume that an initial point $\mathbf{P}_{s,0}$ emits ray vector $\mathbf{v}_{s,0}$ that intersects with target curved surface at one-point $\mathbf{P}_0$ which is used to determine the relative position of secondary reflector. According to the intersection between target point $\mathbf{P}_{t,0}$ and vector $\mathbf{L}_{t,0}$, the normal vector is $\mathbf{n}_0 = \frac{\mathbf{v}_{t,0}}{|\mathbf{v}_{t,0}|} - \frac{\mathbf{v}_{s,0}}{|\mathbf{v}_{s,0}|}$, and the extension of normal vector can be expressed as $\mathbf{v}_0 = \mathbf{P}_0 + \lambda_0 t_0$, where t_0 means the argument.

(2) The second ray vector $v_{s,1}$ emitted from the next point $\mathbf{P}_{s,1}$ is reflected by the local curve and reaches the target point $\mathbf{P}_{t,1}$. One scalar value $\lambda_{s,1}$ will satisfy the intersection of ray $[\mathbf{P}_{s,1}, \mathbf{v}_{s,1}]^T$ with point $\mathbf{P}_1$ [20]:

$$\mathbf{P}_1 = \mathbf{P}_{s,1} + \lambda_{s,1}\mathbf{v}_{s,1} \tag{1}$$

Now, if the value of $\lambda_{s,1}$ is obtained, the position of $\mathbf{P}_1$ can be determined.

(3) Construct segment $\overset{\frown}{\mathbf{P}_0\mathbf{P}_1}$ as a circular curve so that scalar value $\lambda_{s,1}$ can be solved. Note that the normal vectors n_0 and n_1 are perpendicular to the curve, so that the following relation exists [19]:

$$\overline{\mathbf{C}_0\mathbf{P}_0} = \overline{\mathbf{C}_0\mathbf{P}_1} \tag{2}$$

In this formula, $\mathbf{P}_0$ is a known point.

Here, vector v_0 and v_1 intersect at point C_0. v_0 is the single function of argument t_0 and can be obtained using:

$$\mathbf{v}_0 = \mathbf{P}_0 + \mathbf{n}_0 t_0 \tag{3}$$

In the same way, v_1 can be expressed as:

$$\mathbf{v}_1 = \mathbf{P}_1 + \mathbf{n}_1 t_1 \tag{4}$$

where n_1 means the normal vector derived from [21]:

$$\mathbf{n}_1 = \mathbf{Rot}(y, \theta_1)(-\mathbf{v}_{s,1}) \tag{5}$$

Here, emitting vector $\mathbf{v}_{s,1}$ is already known and θ_1 is the bisector angle between incident and reflected vectors calculated from:

$$\theta_1 = \frac{1}{2}\cos^{-1}(-\mathbf{v}_{s,1} \cdot \mathbf{v}_{t,1}) \tag{6}$$

When the scalar value of $\lambda_{s,1}$ is determined, point $\mathbf{P}_1$ and the normal vector n_1 would be achieved by Equations (1) and (5). Based on the same principle, coordinate values of points $\mathbf{P}_2$, $\mathbf{P}_3$, $\mathbf{P}_4$ and corresponding normal vectors can be solved. These points were used together for the forming of a free-form surface. Note that the target points $\mathbf{P}_t$ are special, that need to satisfy the requirements of the PV/thermal combined application. The sampled target points evenly distributed along the width of the PV panel in Figure 2. Some other points are assigned for thermal heat transfer. Based on the energy conservation in radiation heat transfer, the parameter definitions of solar concentrator and receiver satisfy the following relation:

$$k\left(R_{max}{}^2 - R_{min}{}^2\right)/C_G = \left(d_{max}{}^2 - d_{min}{}^2\right) \tag{7}$$

where k and C_G represent the occupation and Geometric Concentration Ratio of the PVR component. R is the radius of primary concentrator and d is the section width of the PVR.

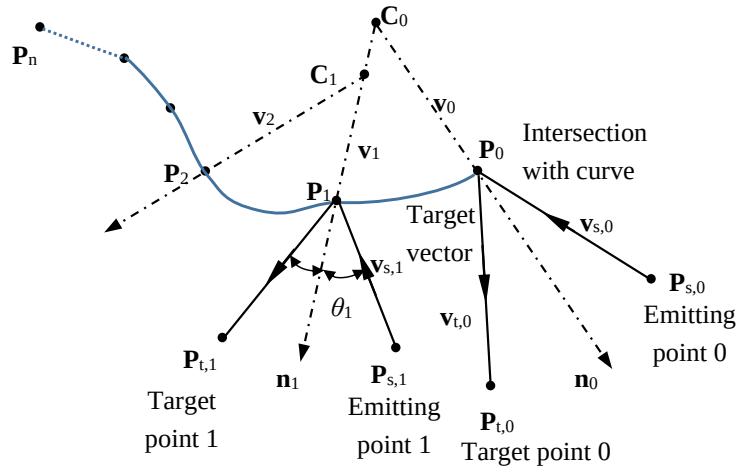

Figure 4. Generating free-form curve using CGCM [19].

The free-form curve is generated based on the whole discrete points. More intensive points obtain higher precision but also more simulation cost for ray tracing. With different points quantity, Figure 5 collected the ray intersections on TR and PVR based on B-spline curve generated by CGCM, and compared them with the preset and accurate target points, through which the accuracy verifications of 10, 30, and 50 points have been conducted. In the figures, lower-sequence points on the left half are used for thermal heat transfer and higher-sequence points on the right half are used for PV conversion. The model aims to collect maximum power at the TR part so the target points are all fixed in original point. It can be seen that, with the increase in points quantity, the constructed model has become more accurate. By considering both precision and simulation cost, 50 discrete points were chosen and generated for the single curve that will be rotated around the central axis for a real free-form surface. The ray tracing technology is then used for the estimation of optical characteristic of TFSC.

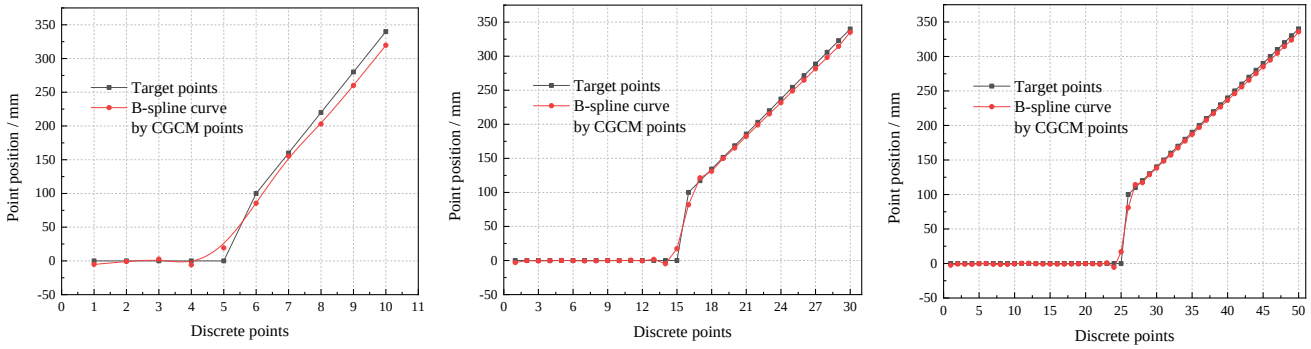

Figure 5. Accuracy verification of generated curve by CGCM. (**a**) 10 discrete points; (**b**) 30 discrete points; (**c**) 50 discrete points.

4. Results

4.1. Verification of Optical Model

To verify the ray tracing model in the current study, the simulated optical efficiency has been compared with the LS3 model [22] at different incident angles, as Figure 6 shows. It can be found that the distributions fit very well. It should be noted that the simulated optical structure remains the same, and solar cone angles for both have not been taken into consideration.

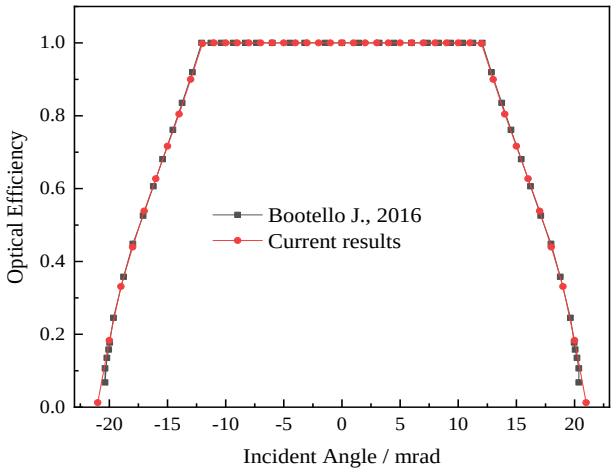

Figure 6. Comparison of optical efficiency between current model and reference [22].

4.2. Forward/Backward Optical Transmission Pattern

It is interesting to firstly discuss the optical transmission of different CPV/T forms. As shown in Figure 7, the forward transmission means the outer region of the concentrator reflects solar rays on the external PV panel, and the inner region reflects rays on the internal thermal tube. By contrary, the backward transmission means two regions of concentrator lead to a crossed ray path corresponding to different receivers with an opposite order of PVR and TR sequence. The geometrical parameters of a simulated TFSC are presented in Table 1. The outer width of PVR was calculated based on the concentration and inner width according to the above Equation (7). The data of calculated points are presented in the Appendix A Table A1.

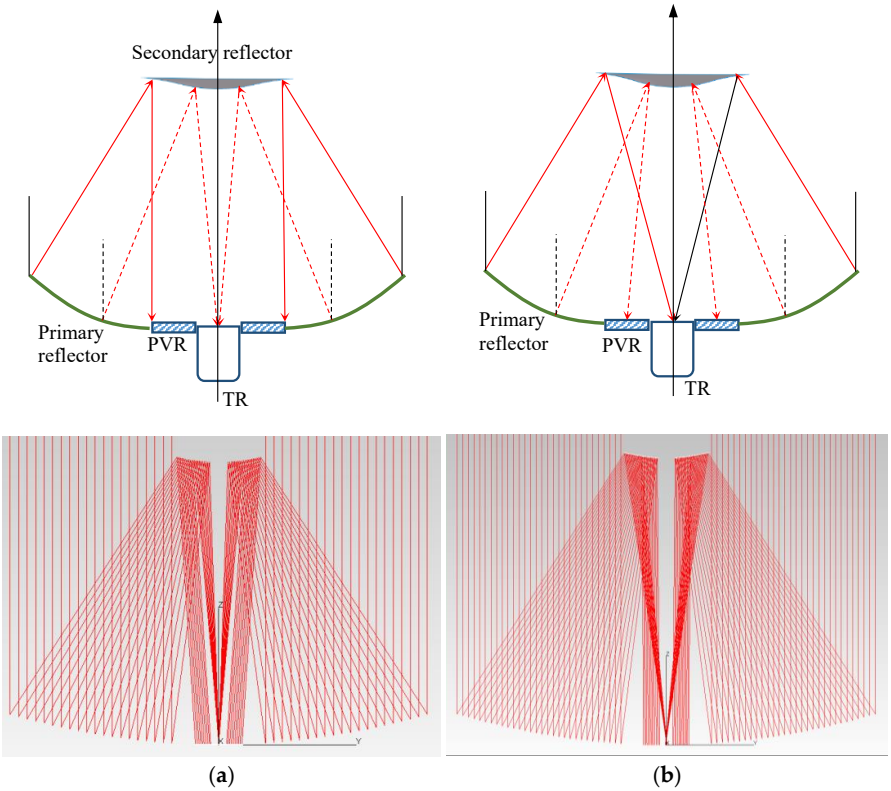

Figure 7. Two different transmission patterns of TFSC. (**a**) Forward transmission. (**b**) Backward transmission.

Table 1. Structural parameters of TFSC for ray-tracing simulations.

Primary Concentrator	Secondary Concentrator	Energy Receiver
Focal length = 5 m, Radius = 3 m, Hole radius = 0.34 m	Section half-length = 0.6 m, TR/PVR divided ratio = 0.5	Height = 0 m, Inner width of PVR = 0.1 m, Outer width of PVR = 0.34 m (predicted), PVR geometry concentration = 5 suns

The optical transmission vectors/incident angles are the main differences between forward and backward models. The relative percentages of radiation energy with incident angles are presented in Figure 5. The simple point sun model cannot satisfy the real working condition of the designed solar concentrator. Therefore, the angular diameter of the sun 32 arc minutes has also been included in the simulation. We can clearly find that the changing trend with incident angles becomes more moderate for the solar angular model compared with the point sun model, meaning that the collected sun rays are more divergent. Under the pattern of forward transmission, we can find in Figure 8 that the most receiving solar rays by PVR are nearly parallel, and this has led to the fact that the peak percentage for the point sun model reached 0.573. The same point for the PVR component is only 0.234 when considering the solar angular effect. The incident angle for TR ranges between 1.25° and 5.75° depending on the cutting edge of the secondary reflector. For backward transmission, the incident solar rays received by PVR present nearly vertical. The rays by TR, however, present a 4.25°–9.25° receiving angle, when the heat loss would be enlarged. At the same design parameters, forward transmission gains more advantages. Therefore, the following work primarily focuses on the forward transmission pattern.

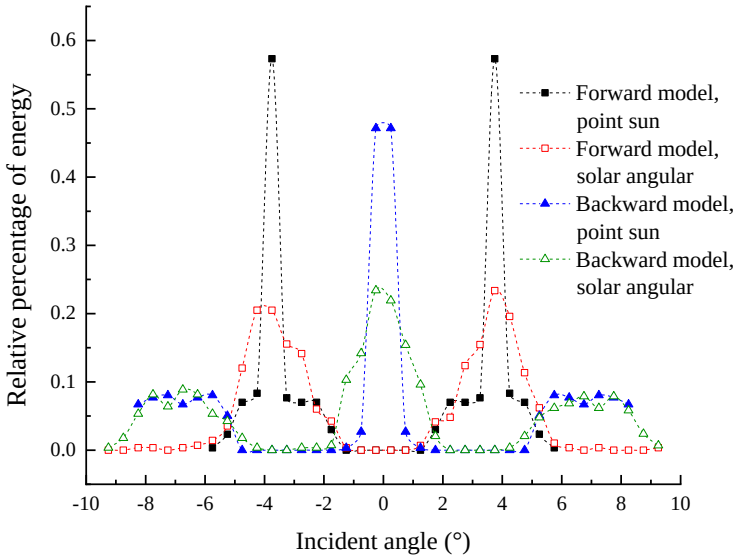

Figure 8. Comparison of the concentrated incident angles between different models.

4.3. Effect of Receiving Position

The height of the receiving component can directly decide the curvature and shape of the secondary free-form surface. This effect has been presented in Figure 9 when the height is between −2 m and ~2 m, and the solar angular effect had been ignored to make it more clear. To avoid the occlusion influenced by PVR to the optical path reflected by the primary mirror, the concentration ratio was set to be 60 suns. As can be seen from this figure, the concentrated solar rays are divided into two parts: some are reflected to the TR in the center, and the others are reflected to the PVR outside. The blank areas between the TR and PVR have become more apparent with the increase of the receiving height; as the optical path is longer, the error caused by discrete points and surface generation dramatically. This can be

easily found in Figure 9d, a ray branch happens at the center of the TR when the height is −2 m, instead of one point at the same position.

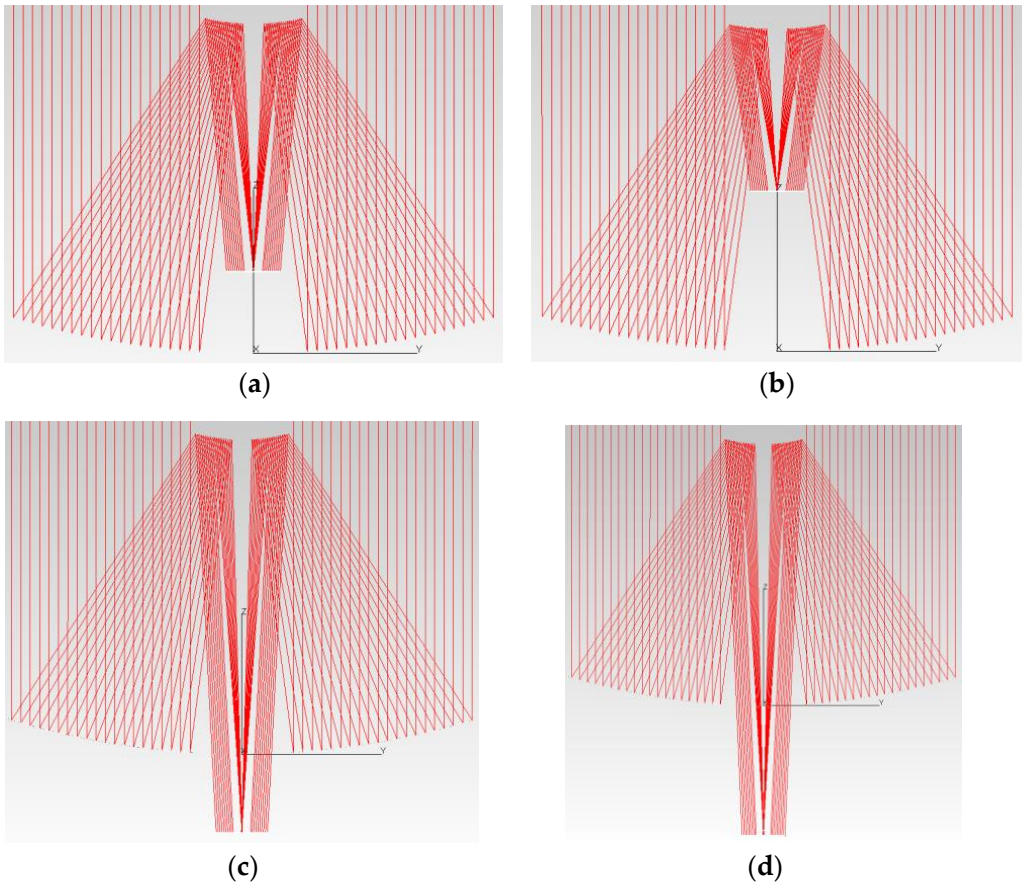

Figure 9. The sketches of ray-tracing paths at different receiving heights between −2 m and ~2 m. (**a**) Receiving height 1 m. (**b**) Receiving height 2 m. (**c**) Receiving height −1 m. (**d**) Receiving height −2 m.

Considering the solar angular angle effect, the distribution of receiving vectors is presented in Figure 10. With the increasing height of the receiver, the incident angle was noticeably enlarged, and the cover range become wider. For instance, when the height is equal to 0 (at the origin point of primary parabola mirror), the incident angle is among 1° to 6°, and the peak is at 3.25°. When the height is 2 m, the incident angle is between 3° to 13°, and the peak is at 7.25°. It should be noted that the incident angle and transition zone meet a compromise. For practical application, the receiver can be located at a lower position to obtain a smaller solar incident angle. At the same time, the overlapped effect for the transition area becomes more obvious and needs to be considered, which increases the risk of overheated/burnout of the PVR.

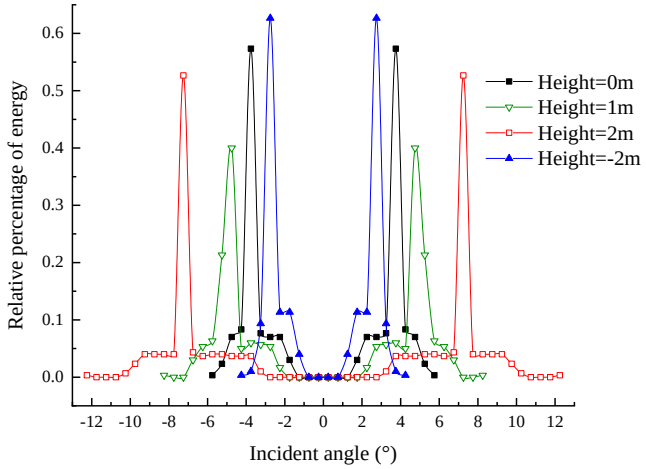

Figure 10. Comparison of the concentrated incident angles at different receiving heights.

4.4. Effect of Different Geometric Concentration Ratios of PVR

The Geometric Concentration Ratio (CG), defined by Formula (7), is an important preset parameter that influences simulated heat flux on PVR. Figure 11 shows the 2-D distributions with different CG targets between 3 and ~20 suns. Concentrated Energy Ratio (CE) is calculated by the receiving heat flux divided by 1000 W/m^2 (one sun energy density). We can find in Figure 11 that the heat flux distribution around the central TR remains the same, and the highest energy concentration ratio reaches 42 suns. For the PVR, the concentrated heat flux distributes uniformly, and the covering size becomes smaller with the increase of the CG values.

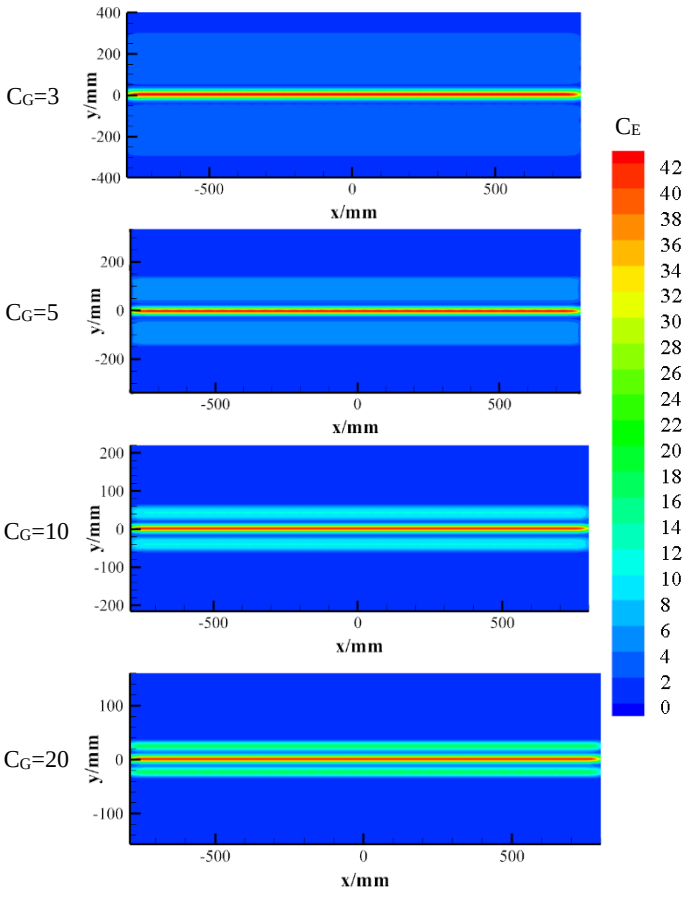

Figure 11. Heat flux distributions at different Geometric Concentration Ratios of PVR.

4.5. Effect of Solar Angular Angle and Tracking Error

A solar angular model with approximately 32 arc minutes' incident divergence will enlarge the receiving size and make the actual CE different with the present concentration of CG. Figure 12a presents the heat flux distribution considering the solar angular angle. The peak solar concentration is much lower compared with the one shown in Figure 11. However, the transient area is becoming fuzzy, which makes the heat flux on both receivers as a continuous distribution. It is predictable that the transient area can be enlarged by moving the preset PVR receiving position outwards. There are some escaped rays from the central hole of the primary trough and hit on the receiver, which make the heat flux on the blank region present as nonzero.

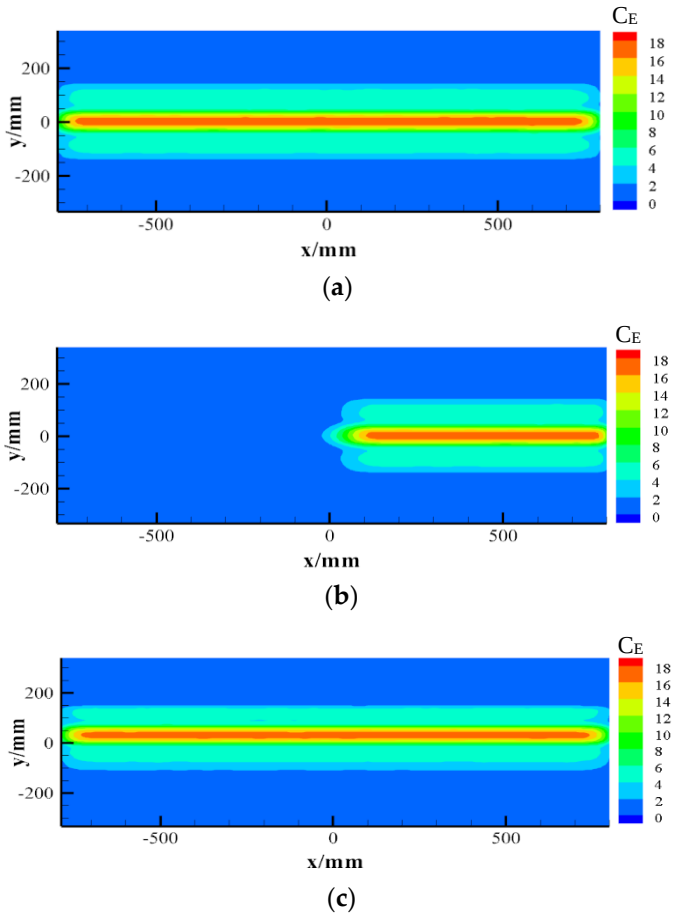

Figure 12. The 2-D heat flux distributions considering solar cone angle with different tracking errors. (**a**) No tracking error. (**b**) Tracking 3° along the x-axis direction. (**c**) Tracking error 3° along the y-axis direction.

A trough-type solar concentrator with 2-D tracking design is usually mounted along a north–south axis and adjusted in real time from the east to the west. When there is no tracking error, the heat flux distribution is presented in Figure 12a. It can be found that the concentration value CE received by PVR is just around the target of 5 suns, and the central thermal receiver collects most of the radiation energy. When the sun rays tilted to the x + direction with a 3° inclination, the entire received heat flux distribution deviated from the left boundary with the length of 900 mm, as Figure 12b shows. In addition, the PV concentrated energy distributes similarly as before in the local receiving region for x > 100 mm. For the TR component, this will lower the heat transfer temperature. For the PVR component, the strategy of series-parallel circuit connections for PV cells needs to be considered.

For the tracking error along another direction in the y-axis, a noticeable influence on heat flux distribution has been revealed in Figure 12c, when the main distribution had been transferred along the y-axis, causing the mismatching problem and even seriously influencing the life expectancy of PVR modules. With a larger tracking error, this mismatch effect will become bigger. Therefore, the tracking error should be strictly controlled for practical applications.

4.6. Effect of PVR Occupation Ratio

The energy allocation for the PV/Thermal proportion of the TFSC system largely depends on the PVR occupation ratio (k = PV part/Total). The radial heat flux distributions with PVR occupation ratios of 0.3, 0.5, 0.7, and 0.9 are shown in Figure 13. Since this is considered in the effect of a solar angular angle, the heat flux steeply dropped at the edge of the TR and PVR components. With the increase of the PVR occupation ratio, this dropping trend on PVR had become more obvious. The main heat flux received by TR is restricted within the radius of 50 mm. The peak concentration drops dramatically with a higher k. It is interesting that the maximum value of PVR exceeds the one of TR when k reaches up to 0.9 and the PV part plays the major role. Figure 14 clearly shows the 2-D heat flux distribution when k = 0.9. The highest concentration is only 8.5× in PVR and the trend is just opposite with Gaussian distribution.

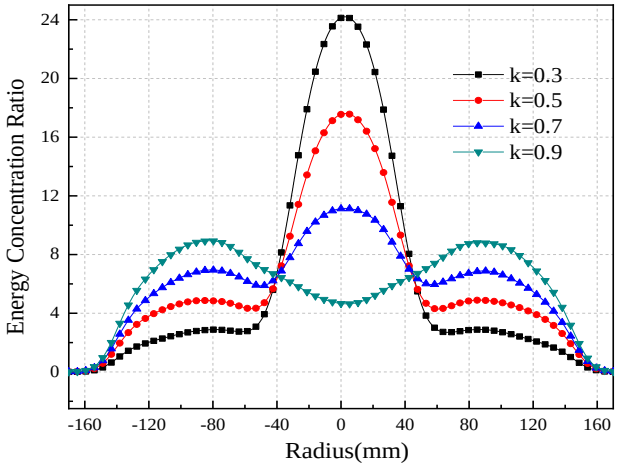

Figure 13. Radial heat flux distributions with different PVR occupation ratios.

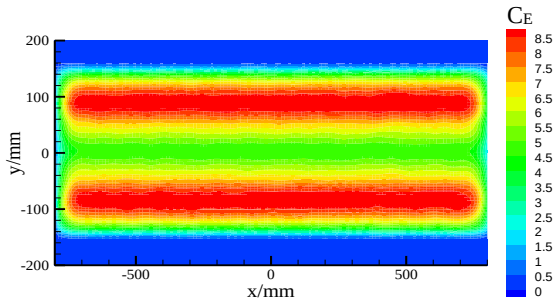

Figure 14. 2-D heat flux distribution when k = 0.9.

5. Discussion

The current study conducted the verification of an optical model and found that the simulated optical efficiency fitted well with the LS3 model at different incidences. From different perspectives, the effects of forward/backward optical transmission, receiving position, different Geometric Concentration Ratios of PVR, solar angular angle and tracking error, PVR occupation ratio have been discussed. It was found that the forward transmission

gains more advantages at the same design parameters. The relative positions of optical structure, energy allocation target and error factors have a substantial impact on the energy distribution and optical efficiency. Therefore, the parameter selection based on the above sensitivity analysis and method is necessary before the practical application of TFSC.

In addition, the ECR distributions in the current model have been compared with reference to show the advantages of TFSC. Figure 15 presents the radial distributions of ECR with different PVR occupation ratios and also the results in reference that simulated for a traditional two-stage solar concentrator [23]. Compared with a normal Gaussian distribution, it can be found that TFSC obtains unique advantages of more obviously separated heat flux regions and also more uniform distribution for PVR. Different k values mainly dominate the proportion allocation of PV and thermal power. The results show that TFSC fitting with hybrid PV/T receivers can better utilize the total Gaussian heat flux.

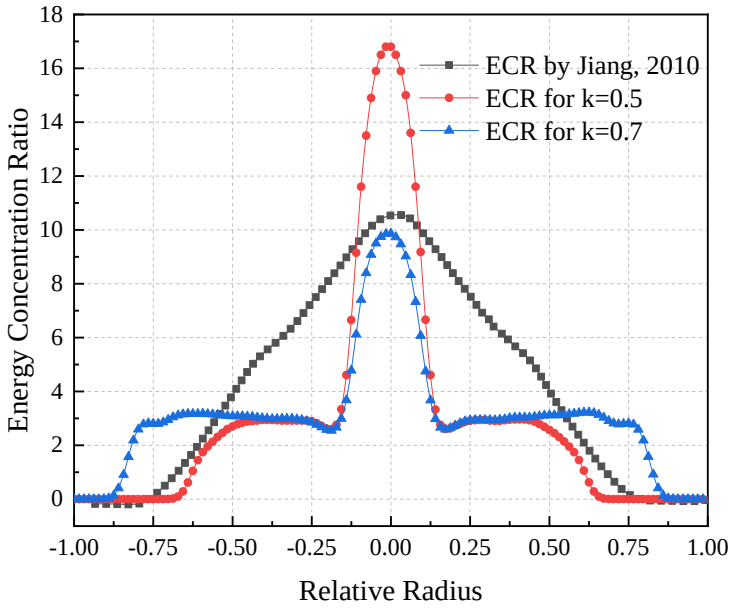

Figure 15. Comparison of ECR distribution in TFSC and Ref [23].

6. Conclusions

The current study proposed a novel trough-type free-form solar concentrator for a PV/Thermal combined application. The TFSC consists of a primary trough concentrator and secondary free-form reflector which was generated by a modified geometric construction method, resulting in a uniform heat flux around the edge region and high concentration at the central receiver. Accuracy verification of the generated curve by CGCM had been conducted to select appropriate discrete points. The optical performance of new designed structure have been verified. Different transmission patterns of TFSC (forward and backward types) have been compared. Afterwards, the effect of Geometric Concentration Ratio of PVR has been investigated. The concentrated heat flux on PV distributes uniformly, and the covering size becomes smaller with the increase of CG values. The existence of solar angular angle makes the peak solar concentration lower, and the transient area becomes fuzzy. The simulation results also show that tracking status and error factor need to be considered carefully for practical applications, and PVR occupation ratio is another key parameter to determine the sharing ratio of PV/Thermal generation. The ECR distributions in the current model had been compared with reference to show the advantages of TFSC. The results show that TFSC fitting with hybrid PV/T receivers can better utilize the total Gaussian heat flux.

The simulation results are promising and significant for the enhancement of trough-type solar concentrator systems. The design model and concept provide references for

improving efficient utilization of concentrated solar radiation and hybrid CPV/T applications with a much higher coolant temperature.

Author Contributions: Conceptualization, X.-l.M.; Data curation, P.Z.; Investigation, F.-P.R.; Software, Z.-x.T.; Supervision, X.-l.M.; Validation, F.-P.R.; Writing—original draft, Z.-x.T. All authors have read and agreed to the published version of the manuscript.

Funding: This work was financially supported through the Foundation Strengthen Project (2021-JCJQ-JJ-0328) and Natural Science Foundation of China (No. 52176205).

Conflicts of Interest: The authors declare no conflict of interest.

Appendix A

The discrete points of secondary free-form surface for the case of Table 1 are as follows, when the initial starting point was (0.6, 4.09) and points number is 50:

Table A1. Generated discrete points of secondary free-form surface.

Point Number	Y Coordinate	Z Coordinate	Point Number	Y Coordinate	Z Coordinate
1	0.6	4.09	26	0.35477	4.03957
2	0.59012	4.0874	27	0.345	4.03828
3	0.58024	4.08485	28	0.33525	4.03703
4	0.57037	4.08235	29	0.3255	4.03581
5	0.56051	4.07989	30	0.31577	4.03463
6	0.55065	4.07749	31	0.30605	4.03349
7	0.5408	4.07513	32	0.29634	4.03239
8	0.53096	4.07282	33	0.28664	4.03132
9	0.52112	4.07056	34	0.27695	4.03028
10	0.51129	4.06835	35	0.26727	4.02929
11	0.50146	4.06619	36	0.2576	4.02832
12	0.49164	4.06407	37	0.24794	4.0274
13	0.48182	4.06201	38	0.23828	4.02651
14	0.47201	4.05999	39	0.22864	4.02565
15	0.46221	4.05802	40	0.219	4.02484
16	0.45241	4.0561	41	0.20937	4.02405
17	0.44262	4.05423	42	0.19975	4.0233
18	0.43284	4.0524	43	0.19014	4.02259
19	0.42306	4.05062	44	0.18053	4.02191
20	0.41329	4.04889	45	0.17093	4.02127
21	0.40352	4.04721	46	0.16133	4.02067
22	0.39376	4.04558	47	0.15174	4.0201
23	0.38401	4.044	48	0.14216	4.01956
24	0.37426	4.04246	49	0.13258	4.01906
25	0.36452	4.04097	50	0.12301	4.0186

References

1. Islam, M.T.; Huda, N.; Abdullah, A.B.; Saidur, R. A comprehensive review of state-of-the-art concentrating solar power (CSP) technologies: Current status and research trends. *Renew. Sustain. Energy Rev.* **2018**, *91*, 987–1018. [CrossRef]
2. Pitz-Paal, R. High temperature solar concentrators. *Sol. Energy Convers. Photoenergy Syst.* **2009**, *1*, 199–241.
3. Dai, G.-L.; Xia, X.-L.; Sun, C.; Zhang, H.-C. Numerical investigation of the solar concentrating characteristics of 3D CPC and CPC-DC. *Sol. Energy* **2011**, *85*, 2833–2842. [CrossRef]
4. Gordon, J.M.; Ries, H. Tailored edge-ray concentrators as ideal second stages for Fresnel reflectors. *Appl. Opt.* **1993**, *32*, 2243–2251. [CrossRef] [PubMed]
5. Friedman, R.P.; Gordon, J.M.; Ries, H. New high-flux two-stage optical designs for parabolic solar concentrators. *Sol. Energy* **1993**, *51*, 317–325. [CrossRef]
6. Kribus, A.; Doron, P.; Rubin, R.; Karni, J.; Reuven, R.; Duchan, S.; Taragan, E. A multistage solar receiver: The route to high temperature. *Fuel Energy Abstr.* **2001**, *42*, 3–11. [CrossRef]

7. Al-Nimr, M.d.A.; Bukhari, M.; Mansour, M. A combined CPV/T and ORC solar power generation system integrated with geothermal cooling and electrolyser/fuel cell storage unit. *Energy* **2017**, *133*, 513–524. [CrossRef]
8. Ries, H.; Gordon, J.M.; Lasken, M. High-flux photovoltaic solar concentrators with kaleidoscope-based optical designs. *Sol. Energy* **1997**, *60*, 11–16. [CrossRef]
9. Liu, Y.; Hu, P.; Zhang, Q.; Chen, Z. Thermodynamic and optical analysis for a CPV/T hybrid system with beam splitter and fully tracked linear Fresnel reflector concentrator utilizing sloped panels. *Sol. Energy* **2014**, *103*, 191–199. [CrossRef]
10. Miñano, J.C.; Benítez, P.; Zamora, P.; Buljan, M.; Mohedano, R.; Santamaría, A. Free-form optics for Fresnel-lens-based photovoltaic concentrators. *Opt. Express* **2013**, *21*, A494–A502. [CrossRef] [PubMed]
11. Miñano, J.C.; Benítez, P.; Santamaría, A. Free-form optics for illumination. *Opt. Rev.* **2009**, *16*, 99–102. [CrossRef]
12. Cvetković, A.; Hernandez, M.; Benítez, P.; Miñano, J.C.; Schwartz, J.; Plesniak, A.; Jones, R.; Whelan, D. *The SMS3D Photovoltaic Concentrator*; SPIE: Bellingham, WA, USA, 2008.
13. Benítez, P.; Miñano, J.C.; Zamora, P.; Mohedano, R.; Cvetkovic, A.; Buljan, M.; Chaves, J.; Hernández, M. High performance Fresnel-based photovoltaic concentrator. *Opt. Express* **2010**, *18*, A25–A40. [CrossRef] [PubMed]
14. Alvarez, J.; Hernandez, M.; Benitez, P.; Minano, J. *TIR-R Concentrator: A New Compact High-Gain SMS Design*; SPIE: Bellingham, WA, USA, 2001.
15. Miñano, J.; Hernández, M.; Benítez, P.; Blen, J.; Dross, O.; Mohedano, R.; Santamaría, A. *Free-Form Integrator Array Optics*; SPIE: Bellingham, WA, USA, 2005.
16. Luo, Y.; Feng, Z.; Han, Y.; Li, H. Design of compact and smooth free-form optical system with uniform illuminance for LED source. *Opt. Express* **2010**, *18*, 9055–9063. [CrossRef] [PubMed]
17. Hernández, M.; Benítez, P.; Miñano, J.; Cvetkovic, A.; Mohedano, R.; Dross, O.; Jones, R.; Whelan, D.; Kinsey, G.; Alvarez, R. *The XR Nonimaging Photovoltaic Concentrator*; SPIE: Bellingham, WA, USA, 2007.
18. Cheng, D.; Wang, Y.; Hua, H. *Free Form Optical System Design with Differential Equations*; SPIE: Bellingham, WA, USA, 2010.
19. Tsai, C.-Y. Improved irradiance distribution on high concentration solar cell using free-form concentrator. *Sol. Energy* **2015**, *115*, 694–707. [CrossRef]
20. Lu, C.-H.; Sung, C.-K. Skew ray tracing and sensitivity analysis of hyperboloid optical boundary surfaces. *Optik* **2013**, *124*, 1159–1169. [CrossRef]
21. Liao, T.-T. A skew ray tracing-based approach to the error analysis of optical elements with flat boundary surfaces. *Optik* **2008**, *119*, 713–722. [CrossRef]
22. Núnez Bootello, J.P.; Price, H.; Silva Pérez, M.; Doblaré Castellano, M. Optical Analysis of a Two Stage XX Concentrator for Parametric trough Primary and Tubular Absorber with Application in Solar Thermal Energy trough Power Plants. *J. Sol. Energy Eng.* **2016**, *138*, 021002. [CrossRef]
23. Jiang, S.; Peng, H.; Mo, S.; Chen, Z.J.S.E.M.; Cells, S. Optical modeling for a two-stage parabolic trough concentrating photovoltaic/thermal system using spectral beam splitting technology. *Sol. Energy Mater. Sol. Cells* **2010**, *94*, 1686–1696. [CrossRef]